Characterization of diatomaceous earth coated with nitrated asphaltenes as superior adsorbent for removal of VOCs from gas phase in fixed bed column

Maksymilian Plata-Gryl [a], Malwina Momotko [a], Sławomir Makowiec [b], Grzegorz Boczkaj [a,c,*]

[a] Gdansk University of Technology, Faculty of Chemistry, Department of Process Engineering and Chemical Technology, G.Narutowicza St. 11/12, 80-233 Gdansk, Poland
[b] Gdansk University of Technology, Faculty of Chemistry, Department of Organic Chemistry, G.Narutowicza St. 11/12, 80-233 Gdansk, Poland
[c] EkoTech Center, Gdansk University of Technology, G.Narutowicza St. 11/12, 80-233 Gdansk, Poland

ARTICLE INFO

ABSTRACT

Asphaltenes isolated from bitumen possess unusual adsorption characteristics that can be further enhanced by chemical modifications to promote interactions with VOCs'. Herein, nitrated asphaltenes are used as an active layer coated on a surface of a diatomaceous earth, in order to prepare an efficient adsorbent (AsfNitro). Breakthrough experiments with benzene, pyridine, and 1-nitropropane revealed significant increase in adsorption capacity, after deposition of nitrated asphaltenes, by 26, 12, and 8 times respectively. The adsorption capacity of AsfNitro for benzene per square meter of surface area is far more superior than for other adsorbents in use. Moreover, the AsfNitro exhibited excellent efficiency. For adsorption of 1-nitropropane and pyridine, almost 100% of the adsorbent's bed was effectively used. Inverse gas chromatography measurements proved that nitrated asphaltenes were exclusively responsible for the adsorption properties, and the role of the diatomaceous earth was only to provide the surface area. Presented findings can be extended to other support materials and their inherent limitations for adsorption of VOCs can be overcome. Comparison of adsorption enthalpies demonstrated that common adsorbents e.g. activated carbons, cannot compete with AsfNitro in terms of sorbate-sorbent interactions. Additionally, contribution of chemisorption mechanism was recognized for AsfNitro, which indicate catalytic properties, and opens a new research field about asphaltenes' novel practical applications. Application of asphaltenes in adsorption processes can be an effective procedure for risk mitigation of hazardous VOCs, accompanied by effective waste management and materials' valorisation. Wasted adsorbent can be easily regenerated (without deterioration of surface properties), or blended in bitumen-aggregates mixes for road paving applications.

1. Introduction

Importance of volatile organic compounds (VOCs) removal from waste gases is obvious due to their often toxic [1], and odorous character [2], as well as participation in atmospheric photochemical reactions [3,4]. Exposure to VOCs emitted from both anthropogenic [5–9], and natural sources [10,11] pose a threat to the respiratory and nervous systems [7,8,11,12]. Regardless of adverse health effects, VOCs pollution has attracted a great public attention because of their capability to cause odour problems [13–15]. This type of pollution is becoming an important environmental issue as it is affecting directly the quality and comfort of human life [16,17], event at low concentrations, which are not necessarily dangerous for physical health.

VOCs emission can be controlled and limited by different techniques [18] e.g.: membrane separation, absorption [19], adsorption [20], condensation [21], catalytic oxidation [22], biodegradation [23], thermal oxidation [24] or plasma catalysis [25]. Among these methods, adsorption is regarded as efficient, feasible, robust and economical approach with straightforward design and mild operating conditions [20,26]. Additionally, it allows to recover and reuse an adsorbent and an adsorptive (VOC) through thermal and/or vacuum desorption [27].

Adsorption is based on interaction between the surface of the adsorbent and the adsorptive, present in the fluid phase, via physical interactions (physisorption) or chemical bonding (chemisorption). The

performance of the adsorption processes is determined by textural properties (surface area, porosity, pore size distribution) and surface functional groups of the adsorbent. While textural properties will provide the adsorption capacity, functional groups will be responsible for the selectivity of adsorption. Adsorbents that are commonly used for removal of VOCs are: activated carbons (ACs), zeolites, hypercrosslinked polymeric resins, and metal organic frameworks (MOFs) [26,28–30].

Since the key parameter in adsorption is the adsorbent, major contributions to the development of this technique were made by the studies on new types of adsorbents e.g. carbon nanotubes [31], graphene [32], MOFs [33]. Significant part of this research is devoted to utilization of waste materials as adsorbents [34,35], since to some extent adsorption takes place on virtually any material. Without a doubt, waste materials in their raw form cannot match AC in terms of adsorption performance, but considering their accessibility and low value they are an interesting alternative for traditional adsorbents, at least in waste gases and wastewater treatment processes.

Asphaltenes are a group of chemical compounds with interesting adsorption properties [36–38], that can fall under the category of waste material. At the present moment their applicability is limited to the paving materials [39,40] – asphaltenes are part of asphalt and bitumen products from oil refineries, and as such asphaltenes can be considered as an unwanted by-product. Generally, they are a source of severe damages to both upstream and downstream oil processing systems, and the oil company's concern is to ensure their separation from process streams, or at least stabilization to prevent uncontrolled precipitation [41,42]. Asphaltenes are the most polar fraction of crude oil with the highest molecular weight. From structural point of view, those are polyromantic hydrocarbons (PAHs) with 4–7 condensed aromatic rings, peripheral alkyl chains, multiple functional groups and heteroatoms - examples of asphaltenes' molecular structure can be found in the Figure S1.

Due to quite complicated structure, asphaltenes are defined on the basis solubility: as a fraction of crude oil insoluble in n–alkanes and soluble in toluene/benzene. The highest content of asphaltenes fraction is observed in asphalts, since non-volatile asphaltenes remains quantitatively in residues from distillation processes. Moreover, during asphalt air blowing processes the structure of asphaltenes is changed by introduction of new oxygen containing functional groups [43–45].

Recently, new emerging applications of asphaltenes have been reported eg.: for adsorption [36–38], catalysis [46], and advanced oxidation processes (AOPs) [47]. In case of adsorption processes, asphaltenes are interesting as contrary to graphene or carbon nanotubes, they are readily soluble in organic solvents. Thus, it is possible to immobilize small amounts of asphaltenes on the surface of materials that possess developed surface area but low adsorption capacity. Proper combination should provide synergistic effect, i.e. strong adsorbent having high surface area.

Moreover the structure of asphaltenes is prone to chemical modifications that can increase their adsorption performance [36,37] and they can be easily isolated from bitumen with high purity [48]. Utilization of asphaltenes in the adsorption processes can be a next step toward effective waste management, waste valorisation and risk mitigation of hazardous VOCs for environment and humans.

In this study an effort was made to test the applicability of diatomaceous earth coated with nitrated asphaltenes for gas purification under dynamic conditions. The adsorption properties were scrutinized by breakthrough curves for VOCs, that are significant environmental pollutants e.g. pyridine (odorous compound), tetrachloroethane (chlorinated hydrocarbon) and benzene (carcinogenic compound) at environmentally relevant concentrations and temperatures. Additionally, the impact of humidity, thermal stability and reusability were tested. The adsorption behaviour between VOCs and nitrated asphaltenes was qualitatively and quantitatively followed by Fourier-transform infrared spectroscopy (FTIR), inverse gas chromatography (IGC) and low

temperature nitrogen adsorption.

2. Experimental

2.1. Asphaltenes isolation and purification

Asphaltenes were isolated from bitumen 20/30 SDA (Lotos Group, Poland) by modified precipitation method followed by additional purification in Soxhlet apparatus, for 24 h at the temperature of boiling point of n-heptane (under reflux). Detailed description of the procedures can be found in [48]. For isolation n–heptane EMPLURA (Merck, Germany) was used. The content of asphaltenes in the isolated fraction was 98% as determined by TLC-FID (thin-layer chromatography with flame-ionization detection). The remaining 2% were highly condensed resins.

2.2. Synthesis of nitrated asphaltenes

Nitrated asphaltenes were synthesized by mixing HNO_3 (65%, 6.4 cm^3, 91 mmol, POCH, Poland) with the stirred solution of asphaltenes (1.59 g) in methylene chloride (50 mL, pure p.a., POCH, Poland). Obtained mixture was refluxed and stirred for 16 h. Afterwards, solvent was removed under reduced pressure (ca. 10 mmHg), residue was suspended in methanol (50 mL, pure p.a., POCH, Poland) and filtered off. The precipitate was washed with methanol (20 mL) and dried under vacuum at 80 °C for 8 h. Effects of modification were studied by the FTIR spectroscopy.

Elemental analysis of the nitrated asphaltenes was performed with the Flash 2000 elemental analyser (Thermo Scientific, USA).

2.3. Adsorbent preparation

The KG adsorbent (Kieselgur – diatomaceous earth, 60–80 mesh, Merck, Germany) was used as received from supplier. The AsfNitro adsorbent was prepared using the methods of coating of stationary phases onto solid support. Before coating, the support (KG) was washed with methanol (pure p.a., POCH, Poland) and deionized water, followed by activation in the vacuum drier at 200 °C for 5 h. Next, the support was cooled and transferred to the previously prepared solution of asphaltenes in dichloromethane (pure p.a., POCH, Poland). The amount of nitrated asphaltenes and KG was adjusted to give the final asphaltenes content of 10% m/m. The mixture was mixed in a flask and the solvent was evaporated in a rotary evaporator. After removal of the solvent, the prepared adsorbent, named AsfNitro, was dried in the vacuum drier at 105 °C for 1 h.

Dichloromethane was used for the deposition/immobilization of nitrated asphaltenes on the KG according to our previous practice in this field. It was fully recovered from the rotary evaporator. However, as this compound is considered a hazardous to the environment, in industrial practice it can be substituted by other solvents providing solubility of nitrated asphaltenes e.g. toluene.

2.4. Fourier-transform infrared spectroscopy analysis

Chemical structure of the prepared AsfNitro adsorbent before and after adsorption of target VOCs was determined using Fourier transform infrared spectroscopy (FTIR), performed on a Nicolet Spectrometer IR200 (Thermo Scientific, USA). The device was equipped with attenuated total reflectance (ATR) attachment with diamond crystal. Measurements were made with 1 cm^{-1} resolution in the range from 4000 to 400 cm^{-1}.

2.5. Surface area measurement

Nitrogen adsorption–desorption isotherms (BET method for the calculation of the specific surface area) were recorded using the Micromeritics Gemini V (Norcross, USA) instrument at 77 K (liquid

nitrogen temperature).

2.6. Inverse gas chromatography measurements

IGC measurement were conducted using a Clarus 580 gas chromatograph (Perkin Elmer, USA) with a flame ionization detector (FID). The instrument was interfaced to a PC computer for control and acquisition of chromatograms in TotalChrom 6.3.2 application (Perkin Elmer, USA). Adsorbents were packed into GC stainless steel columns (inner diameter 2.1 mm, length 20 cm) using dry packing method, and were preconditioned twice in a gas chromatograph by passing carrier gas (N5.0 nitrogen, Linde Gas, Poland) in the temperature program (5 min @ 50 °C, 2 °C/min, 120 min @ 250 °C). The flowrate of the nitrogen was set to 20 mL min^{-1}. All test compounds were used as received from supplier, and are listed in the Table S1 together with their basic properties. Methane was used as non-interacting marker to determine void time of columns. The retention time of test probes was determined at peak maximum.

IGC at infinite dilution (IGC-ID) was used to measure: free energy of adsorption (ΔG_A), dispersive (γ_S^D), and specific (γ_S^{SP}) components of the surface free energy, electronacceptor (γ_S^+), and electrondonor (γ_S^-) parameters of a solid's surface. Based on the values of ΔG_A the enthalpy of adsorption (ΔH_A) for test probes was calculated. IGC at finite concentration (IGC-FC) was used to measure sorption isotherms for selected probes. Details of the IGC's experimental methods and calculations are given in the SI – section S1 and S2.

2.7. Breakthrough measurements

Breakthrough curves were measured on a modified Autosystem XL gas chromatograph (Perkin Elmer, USA) with an online FID detection, using 20 cm (2.1 mm inner diameter) long stainless steel columns. As a model contaminants, mixtures of benzene, pyridine and 1-nitropropane in nitrogen were used. All three are representatives of VOC group and their concentration in the air is limited. Benzene is known for its carcinogenic properties, pyridine is an odorous compound with very low odour threshold, and 1-nitropropane is a flammable, odorous, and very volatile compound. Moreover, 1-nitropropane possess a threat of explosion when mixed with air and/or when it is in contact with acids, bases, oxidizing agents or heavy metal oxides [49].

Initial concentrations for benzene, pyridine, and 1-nitropropane were 9.6, 46.5, 275 ppm, respectively. Mixtures were prepared in separate gas cylinders and their concentration was determined by GC-FID technique. The initial concentration of test species were set to be 10 times higher than permissible exposure limit (PEL) in the workplace during an 8 h workday as set by the U.S. Occupational Safety and Health Administration [49]. The aim was to collect reliable data about adsorption performance without artificial exaggeration of adsorption performance of the AsfNitro adsorbent, as very often the unrealistic high concentration of test compound can amplify the adsorption capacity.

Measurements were conducted on two relative humidity (RH) levels, i.e. 5 and 80%, to evaluate the influence of low and high levels of water in the gas stream on adsorption performance. RH level was measure by HM2301 humidity sensor (Hanwei, China). Experiments at RH = 80% were performed by sweeping vapours from above the water placed in a heated container.

All measurements were performed at 30 °C and at 30 mL min^{-1} flow rate. Breakthrough point was set to $\frac{C_t}{C_0} = 0.1$, where C_t (mg L^{-1}) is the outlet gas concentration at given time and C_0 (mg L^{-1}) is the influent concentration. Maximum adsorption capacity Q_{max} (mg g^{-1}) of an adsorbent was calculated as follows:

$$q_{max} = F \int_{t=0}^{t_e} \frac{(C_0 - C_t)dt}{m} \tag{1}$$

Where m (g) is the mass of the adsorbent, and t_e (min) is the exhaustion

time at $\frac{C_t}{C_0} = 0.95$. Breakthrough adsorption capacity Q_{break} (mg g^{-1}) was calculated from the same equation by changing the integral bound from t_e to t_b (breakthrough time at $\frac{C_t}{C_0} = 0.1$).

Breakthrough volume $BTV_{10\%}$(L) was calculated according to Eq. (2):

$$BTV_{10\%} = \frac{Ft_b}{1000m} \tag{2}$$

The effective adsorption capacity Q_{eff} (mg g^{-1}) is defined as a part of adsorption capacity utilized up to the breakthrough point and was calculated as:

$$Q_{eff} = \frac{Q_{break}}{Q_{max}} \cdot 100 \tag{3}$$

The mass transfer zone MTZ (cm), i.e. a part of packed bed where adsorption takes place, and length of unused bed LUB (cm), i.e. a distance of the adsorbent bed, that is not saturated at the breakthrough time were calculated as follows:

$$MTZ = L\left(\frac{t_e - t_b}{t_e}\right) \tag{4}$$

$$LUB = L\left(\frac{t_s - t_b}{t_s}\right) \tag{5}$$

where t_s (min) is the time at which $\frac{C_t}{C_0} = 0.5$.

2.8. Regeneration ability

The regeneration ability of the AsfNitro was tested with benzene. After saturation, the adsorbent was regenerated by thermal desorption. A N$_2$ stream was passed through the column with a 30 mL min^{-1} flowrate, at 200 °C until the detector's signal after the desorption stage was stable. Next, the adsorbent was reused to measure the adsorption capacity. Mentioned procedure was repeated 10 times.

2.9. Quality assurance of data

All data points obtained by GC measurements and presented in this paper are an average of three injections. To minimize error caused by linearization of the isotherm and breakthrough curve models, experimental data were fitted by non-linear regression. Computations were performed by R programming language [50] using the Levenberg-Marquardt non-linear least-square algorithm provided by the MINPACK library [51].

Although, data was fitted to the nonlinear forms of the isotherm and breakthrough curve models, the goodness of fit was evaluated by both: the Chi-square coefficient X^2, and the R^2, as the R^2 is more instinctively comprehended:

$$X^2 = \frac{\sum (y_e - y_c)^2}{y_c} \tag{6}$$

$$R^2 = \frac{\sum \left(y_c - \overline{y}_e\right)^2}{\sum \left(y_e - \overline{y}_e\right)^2} \tag{7}$$

where y_c, y_c, and $\overline{y}_e$ are values calculated by a model, experimental, and experimental mean, respectively.

3. Results and discussion

For preparation of the adsorbent with nitrated asphaltenes, the Kieselgur was used as a support. Kieselgur, also known as diatomite or diatomaceous earth, is a fossil material made from siliceous (mainly amorphous hydrated silica) skeletons of diatoms. It was chosen for

several reasons: 1) it is a low-cost material, as the diatomaceous silica is the most abundant form of silica known, 2) it has highly developed bimodal (macro and meso) porosity which makes it a popular adsorbent (mesopores enhance the specific surface area and macropores facilitates the mass transport and diffusion), 3) it has high mechanical and chemical resistance, and 4) the rigid structure of diatomite particles allows to maintain a high filtering velocity and avoid blocking of the filter with tiny solid particles, if present in the processed stream. It is also noteworthy to mention that some attention was already paid to modifying the surface of diatomite to improve its adsorption properties [52,53]. The proof of successful modification leading to introduction of –NO$_2$ groups to the structure of asphaltenes can be found in our previous study and in the Figure S1 [36]. Also, the elemental composition of raw and nitrated asphaltenes proved the fact of successful modification. The nitrogen content increased from 1.28 to 6.25% wt., and oxygen from 1.79 to 18.81% wt. Analysis of the results reveals that –NO$_2$ groups account for 16.40% wt. of nitrated asphaltenes (0.0036 mol of –NO$_2$ per gram). The molar ratio of introduced oxygen and nitrogen (O/N) equal to 3 indicate that apart from –NO$_2$ groups, also other oxygen-containing groups were added to the structure of asphaltenes, because of oxidation. It is in line with the results of FTIR published previously [36]. At the same tame molar ratio of C/H, for both raw and nitrated asphaltenes is close to 1. It is a typical value for asphaltenes, and demonstrates their high aromaticity.

The low temperature nitrogen adsorption revealed that textural properties of both adsorbents were similar. Neither the BET surface area, nor the total pore volume was changed by the deposition of nitrated asphaltenes on the surface of diatomaceous earth (KG). The BET surface area of the KG and the AsfNitro was 1.480 ± 0.020 and 1.491 ± 0.037 m^2 g^{-1}, respectively. The total pore volume was the same for both adsorbents i.e. 0.0015 cm^3 g^{-1}. It proves that KG, and other similar mesoporous materials, can be a suitable support and surface area provider for asphaltenes.

To evaluate adsorption properties of the adsorbent, the equilibrium (isotherms) and dynamic (breakthrough curves) experiments has been conducted with pyridine, benzene, and 1-nitropropane.

3.1. Breakthrough curves

In real life applications adsorption processes are usually operated under dynamic conditions (i.e. continuous flow of contaminated gas), and with formation of multilayer adsorption. Breakthrough analysis is the method to assess the applicability of the prepared adsorbent through characterization of adsorption capacity, kinetics and selectivity. Breakthrough experiments were performed with controlled temperature of 30 °C in a practical flow-through configuration that mimics conditions used in industrial separations. Fig. 1 presents breakthrough curves for low humidity gas stream (RH = 5% ± 2). Breakthrough curves revealed significant change in the adsorption capacity for all test compounds in favour of AsfNitro adsorbent. The highest change was observed for pyridine and benzene. Interesting observation was made about the shape of the curve for benzene and AsfNitro adsorbent. It is clearly less steep compared to curve for KG. The steepness of the curve is correlated to the efficiency of the adsorption and effective usage of the adsorbent. The more steep is the curve, the smaller width of the mass transfer zone (zone with the highest mass transfer speed) is. More slanted curve may indicate that there is a change in heterogeneity of the surface between KG and AsfNitro. The adsorption centres for benzene may have a wider adsorption potential distribution compared do pyridine and 1-nitropropane. More information about adsorption process were obtained from parameters derived from breakthrough curves that describe performance of columns at RH = 5%, and are presented in the Table 1.

BTV$_{10\%}$, Q$_{max}$, and Q$_{break}$ parameters characterize the adsorption capacity of the adsorbent, which is considerably superior for AsfNitro adsorption capacity compared to KG, regardless of the test compound. In case of waste gas purification, especially important is the substantial
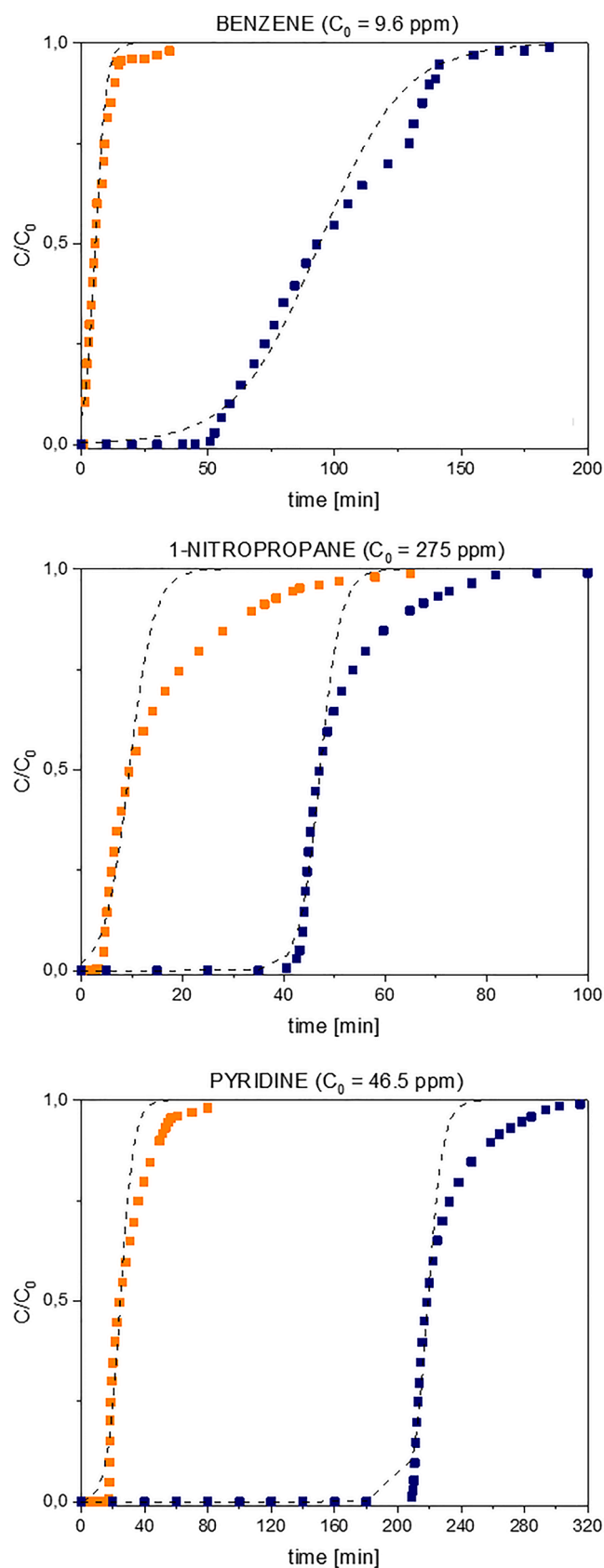

Fig. 1. Breakthrough curves of benzene, pyridine and 1-nitropropane on the KG (■) and AsfNitro (■) adsorbent. Dashed line (– – –) represents logistic growth model. Relative humidity of gas stream was 5%.

Table 1

Operational parameters of investigated columns (with KG and AsfNitro adsorbents) used for adsorption of benzene, pyridine and 1-nitropropane, measured at RH = 5%.

Parameter	$BTV_{10\%}$	Q_{max}	Q_{break}	Q_{eff}	MTZ	LUB
Unit	[L g^{-1}]	[mg g^{-1}]	[mg g^{-1}]	[%]	[cm]	[cm]
benzene						
KG	0.46 ± 0.03	0.048 ± 0.003	0.014 ± 0.001	29.4 ± 3.8	17.3 ± 0.4	12.1 ± 1.1
AsfNitro	12.07 ± 0.77	0.570 ± 0.060	0.360 ± 0.040	68.7 ± 6.6	11.0 ± 0.5	4.3 ± 0.4
pyridine						
KG	3.61 ± 0.21	0.924 ± 0.013	0.544 ± 0.031	58.8 ± 2.5	14.2 ± 0.6	5.4 ± 0.2
AsfNitro	43.86 ± 1.17	7.084 ± 0.210	6.608 ± 0.177	92.3 ± 0.3	4.5 ± 0.3	0.7 ± 0.1
1-nitropropane						
KG	1.10 ± 0.07	3.277 ± 0.127	1.096 ± 0.066	33.4 ± 0.7	17.6 ± 0.1	9.9 ± 0.1
AsfNitro	9.28 ± 0.09	11.045 ± 0.125	9.272 ± 0.091	84.0 ± 1.8	8.7 ± 0.6	1.4 ± 0.1

Table 2

Meaning of the *a* and *b* parameters in regard to the breakthrough curve's models.

Model	Logistic growth function	
	a	b
Yoon-Nelson	$k_{YN}\tau$	k_{YN}
Thomas	$\dfrac{k_T q_0 m}{F}$	$k_T C_0$
Bohart-Adams	$\dfrac{k_{BA} N_0 L}{u}$	$k_{BA} C_0$
Parameter	**Definition**	**Unit**
k_{YN}	Yoon-Nelson rate coefficient	min^{-1}
τ	time required for 50% breakthrough	min
k_T	Thomas rate coefficient	cm^3 mg^{-1} min^{-1}
q_0	maximum adsorption capacity	mg g^{-1}
F	volumetric flowrate	cm^3 min^{-1}
m	mass of the adsorbent	g
k_{BA}	Bohart-Adams rate coefficient	cm^3 mg^{-1} min^{-1}
N_0	adsorption capacity of the adsorbent per unit volume of the bed	mg cm^{-3}
L	bed depth	cm
u	superficial velocity	cm min^{-1}

increase of the breakthrough adsorption capacity (Q_{break}) and breakthrough volume ($BTV_{10\%}$). Higher value of $BTV_{10\%}$ is advantageous as it increases the adsorbent bed service life, and simultaneously decreases required adsorbent mass.

Beside enhancement of adsorption capacity, analysis of breakthrough curves revealed the improvement of the adsorption efficiency. The mass transfer zone (MTZ) reduced after modification of KG with nitrated asphaltenes. The shorter the MTZ, the better the performance of adsorption column. The adsorbent bed was used more effectively leading to a shorter length of unused bed (LUB) – a portion of adsorbent bed that was not exhausted when breakthrough was observed. To give better idea about the efficiency change, the effective adsorption capacity (Q_{eff}) was calculated, i.e. the part of adsorption capacity that was used before the breakthrough occurred. It was two times higher for AsfNitro compared to KG. That value was outstanding for pyridine and 1-nitropropane. AsfNitro adsorbent was exhausted in 92 (pyridine) and 84% (1-nitropropane) when the breakthrough was observed. It is around two times higher than for KG adsorbent. The fact of improved adsorption efficiency is certainly not without significance for the economics of the adsorption process.

The breakthrough data was modelled by three popular mathematical expressions i.e. Bohart-Adams, Thomas and Yoon-Nelson. However, to estimates the values of those parameters a logistic equation was used:

$$\frac{C}{C_0} = \frac{1}{1 + \exp(a - bt)} \tag{8}$$

the definition of *a* and *b* parameters, in regard to the Bohart-Adams, Thomas and Yoon-Nelson models, is presented in the Table 2. The abovementioned approach is applicable, because at the ground level all three mentioned models are one and the same, just with different definitions for *a* and *b* parameters, and can be expressed as the logistic growth function with two parameters [54].

Table 3 summarizes the results of logistic growth model fitting, including calculated values of abovementioned models. Although, experimental curves for both adsorbents where fairly well described by the logistic growth equation, regression analysis derived from Eq. (8) of the experimental breakthrough data obtained for test probes gave better agreements with the AsfNitro's breakthrough curves. It is reflected by the difference between measured and calculated values of τ, q_0, and N_0. For AsfNitro it was below 10%, which is an acceptable agreement of results for such purpose.

The values of models' constants revealed that modification of KG with asphaltenes didn't change significantly the kinetics, except for benzene. For that compound a substantial decrease of k_{YN}, k_T, and k_{BA} was observed. It was expected based on the analysis of the breakthrough

curve's shape. Nitrated asphaltenes on the surface of KG have introduced large number of new active centres with wide distribution of adsorption potential compared to pure KG. As the most active centres are progressively occupied towards the less active, the enthalpy of adsorption decrease. This is illustrated as a decrease in the gradient of the breakthrough curve of benzene on the AsfNitro adsorbent (Fig. 3). Overall, the drop in the rate of benzene adsorption is fully compensated by large increase of adsorption capacity.

The adsorption performance of AsfNitro adsorbent toward benzene was compared with other adsorbents reported in the literature in terms of 10% breakthrough capacity (Q_{break}). Data for 1 Pa inlet partial pressure was extracted from [30]. In this work nitrated asphaltenes are intended to be used as an active layer used to coat a surface area of an inexpensive support. As such, the adsorption capacity will depend on the choice of the support. To highlight it, Fig. 2 was prepared where Q_{break}, measured at RH = 5%, was normalized against the specific surface area of the adsorbents. The adsorption capacity per meter square of surface area is superior to all other adsorbents listed. Results in the Fig. 2 points out the direction for further development of nitrated asphaltenes-based adsorbents – search for materials with suitable surface area e.g. natural minerals, clays, or rocks that are easily available in the target destination. Small particles of inorganic support covered with asphalthenes can be easily utilized. As asphalthenes are a component of bitumen used for road paving applications as well as sealants – the wasted adsorbent bed can be blended with bitumen during preparation of bitumen-aggregates mix. In case of hot mix operations under controlled conditions it would be possible to desorb the VOCs and treat them by proper technology, while wasted adsorbent incorporation as asphalt component. This approach is already used for utilization of post-process ashes which are blended with asphalt.

To test the effect of water vapour on adsorption, measurements at 80 ± 2% relative humidity were performed for benzene and 1-nitropropane. Collected data revealed that the relative humidity had a negative influence on the breakthrough curves. Table S2 lists breakthrough parameters of columns operated under humid conditions.

The breakthrough adsorption capacity decreased under humid conditions. This drop can be attributed to the competitive adsorption of water molecules on the surface of adsorbents. The AsfNitro adsorbent bed become depleted by benzene and 1-nitropropane about 6 and 2 times faster, respectively, compared to dry conditions. The drop of adsorption capacity toward benzene was similar as for e.g. activated carbon prepared from peat [55]. Nevertheless, the AsfNitro retains

Table 3

Results of logistic growth model fitting.

|	k_{YN}(min^{-1})	τ(min)	k_T(cm^3 mg^{-1} min^{-1})	q_0(mg g^{-1})	k_{BA}(cm^3 mg^{-1} min^{-1})	N_0(mg cm^{-3})	$X^2(R^2)$
KG							
benzene	0.473 ± 0.026	5.6 ± 0.1	15458 ± 852	0.037 ± 0.001	15458 ± 852	0.007 ± 0.001	0.366 (0.979)
pyridine	0.239 ± 0.017	24.8 ± 0.2	1583 ± 112	0.804 ± 0.001	1583 ± 112	0.162 ± 0.001	0.850 (0.960)
1-nitropropane	0.413 ± 0.027	9.5 ± 0.1	413 ± 27	2.046 ± 0.004	413 ± 27	0.412 ± 0.001	0.684 (0.961)
AsfNitro							
benzene	0.061 ± 0.002	94.1 ± 0.1	1993 ± 76	0.619 ± 0.001	1993 ± 76	0.125 ± 0.001	0.338 (0.985)
pyridine	0.213 ± 0.015	219.0 ± 0.2	1411 ± 96	7.113 ± 0.005	1411 ± 96	1.433 ± 0.005	0.492 (0.975)
1-nitropropane	0.492 ± 0.033	47.2 ± 0.1	492 ± 33	10.157 ± 0.004	492 ± 33	2.047 ± 0.002	0.399 (0.973)
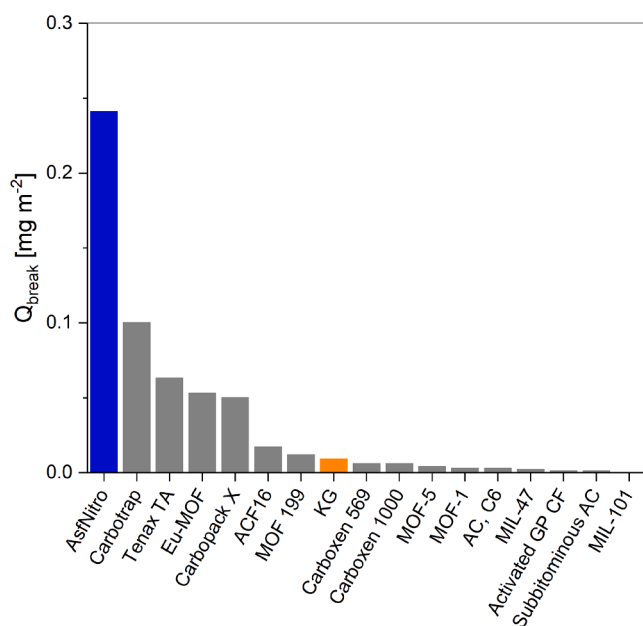
Fig. 2. Adsorption capacities (Q_{break}, breakthrough adsorption capacity), measured at RH = 5%, of AsfNitro, KG and other adsorbents for benzene per surface area of an adsorbent.
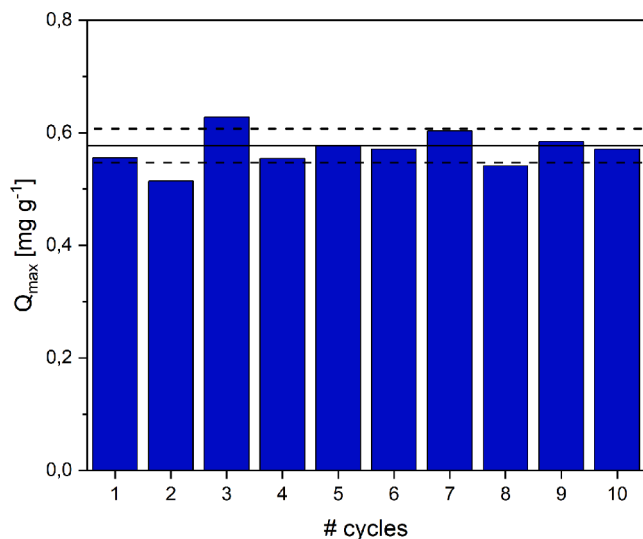

Fig. 3. Reusability of AsfNitro adsorbent for benzene adsorption. Solid line represents mean value, dotted line standard deviation.

partially its favourable adsorption properties.

The reuse potential of the AsfNitro adsorbent was evaluated by monitoring the changes of Q_{max} value for benzene between consequent adsorption–desorption cycles. The regeneration of adsorbent bed was achieved by thermal desorption at 250 °C in pure nitrogen stream. The relative humidity of gas stream, for both adsorption and desorption step, was 5 ± 2%. The results are presented in the Fig. 3.

The AsfNitro represents satisfactory reusability. The maximum adsorption capacity was stable in the course of the 10 consequent adsorption–desorption cycles. The RSD for measured values was around 5%. Moreover, the mentioned result indicate a favourable thermal stability of the AsfNitro, since it was regenerated by the thermal desorption (250 °C). In process scale the desorption can be aided by vacuum, and performed in lower temperatures. It will extend the life cycle of the AsfNitro adsorbent.

Moreover, the adsorption–desorption stability of the adsorbent's performance demonstrates the durability of the chemical modification with –NO$_2$. It is further supported by IGC results, presented in the next sections. After each analysis, adsorbent was thermally regenerated to ensure full desorption of a test probe, and the accuracy of the IGC results indicate that it did not affect the surface properties of AsfNitro.

3.2. Inverse gas chromatography

Both tested adsorbents have similar surface area and porosity. Thus, it can be concluded that the differences in the adsorption performance, observed in breakthrough experiments are not caused by the differences in textural properties and diffusion, but are the result of the different strengths of adsorbate-adsorbent interactions. Those interactions arise from chemical structure of the surface and presence of the specific sorption sites. It leads to preferential adsorption of certain compounds over others. To investigate in detail the thermodynamic equilibrium separation mechanism, the IGC technique was used. In the Table S2 the ΔG_A, ΔH_A and ΔS_A value for all test probes are reported.

3.2.1. Adsorption isotherms

The adsorption isotherms were used to reveal the relationship between the equilibrium concentration in the gas phase and the amount of VOC adsorbed on the surface of KG and AsfNitro adsorbents at low surface coverage ($\theta < 1$). The adsorption equilibrium data were fitted to two well-known isotherm models, to evaluate their utility and to simulate the experimental data. Measurements were done for the same test probes as in breakthrough experiments. The equilibrium adsorption properties were compared in the temperature range between 100 and 140 °C.

Langmuir model is the most extensively used isotherm model. It assumes that adsorption is limited to a one molecular layer, all adsorption sites on the surface are energetically identical, and there is no interaction between adsorbate's molecules [56]. Langmuir model is described by Eq. (9):

$$q_e = q_0 \frac{K_L P}{1 + KP} \tag{9}$$

where q_0 (mg g^{-1}) is the maximum adsorption capacity of the adsorbent, K_L (Pa^{-1}) is the Langmuir equilibrium constant related to the heat of adsorption, and P (Pa) is the partial pressure of the adsorbate in gas phase.

The Freundlich isotherm is an empirical model applicable to adsorption process on heterogeneous surface [57]. The equation for Freundlich model is as follows:

$$q_e = K_F P^{\frac{1}{n}} \tag{10}$$

where K_F (mg g^{-1} Pa$^{-1/n}$) is the parameter related to the adsorption capacity, parameter n (-) characterizes the heterogeneity of the adsorbent's surface and the adsorption intensity. The lower the value of n, the more favourable is adsorption.

Using values of K_L for different temperatures, the heat of adsorption can be estimated from the following van't Hoff equation, which relates the Langmuir equilibrium constant to the temperature [58]:

$$K_L = K_0 exp\left[\frac{-E_A}{RT}\right] \tag{11}$$

where E_A (J mol^{-1}) is the activation energy of adsorption and K_0 is the adsorption equilibrium constant. The relation between the lnK_L and $\frac{1}{T}$ are given in the SI (Figure S4).

Due to very low retention of benzene on KG, the isotherm was measured only for 100 °C and the E_A value couldn't be calculated for that adsorbate-adsorbent pair. For pyridine and 1-nitropropane it was 12.21 ± 1.54 and 3.89 ± 0.14 kJ mol^{-1}, respectively. For AsfNitro the E_A values for benzene, pyridine and 1-nitropropane were 59.94 ± 2.99, 47.85 ± 4.55 and 29.55 ± 3.63, respectively. It is evident that adsorption performance of AsfNitro originates exclusively from presence of nitrated asphaltenes. The E_A increased almost 4 times for pyridine, and over 7 times for 1-nitropropane. For benzene it would be even greater. The magnitude of E_A indicates the character of adsorption i.e. physisorption or chemisorption. Typically, range 5–40 kJ mol^{-1} corresponds to a physisorption and 40–800 kJ mol^{-1} to a chemisorption [59], however that distinction is not rigid.

Values of adsorption energy for AsfNitro falls between two mentioned ranges. It suggest that test probes are bounded to the surface of AsfNitro by synergistic combination of very strong physical interactions and chemical interactions with functional groups on the surface. Before deposition of asphaltenes on the KG's surface the fundamental interacting force were of van der Waals type, and the adsorption process was based solely on physisorption.

To model the experimental data, the Langmuir and Freundlich adsorption isotherm models were used. Full set of results, together with examples of adsorption isotherms at 100 °C, can be found in the SI (Table S3 and Figure S5). The Freundlich model was more adequate for experimental data, however both models explained it correctly, as indicated by high R^2 values. Those results mean that the surface of both adsorbents is not homogenous in terms of adsorption centres' energy. It is further supported by the results presented in the section 3.2.2. Moreover the n values, for all test probes, are lower for AsfNitro adsorbent, meaning more favourable adsorption.

In the Fig. 4 monolayer adsorption capacities, derived from Langmuir model, are compared. The deposition of nitrated asphaltenes on the surface of KG enormously enhanced its adsorption capacity. Generally, the extent of Q_{mono} of test compounds is following the boiling point i.e. the compound with the highest boiling point has the highest monolayer adsorption capacity. For 1-nitropropane, and benzene at 100 °C, the difference between Q_{mono} of adsorbents was around 70 times in favour of AsfNitro, and was quite stable in the whole range of temperature. For pyridine, the difference increases with temperature. From 79 at 100 °C, to 92 times more at 140 °C. It suggests that interactions between pyridine and KG weaken faster with temperature increase, comparing to pyridine and AsfNitro. Less rapid reduce of strength of interactions is favourable for the stability and predictability of the adsorption process.

3.2.2. Surface's heterogeneity

Surface's energy heterogeneity was described by the adsorption potential distribution, which was calculated from the sorption isotherm
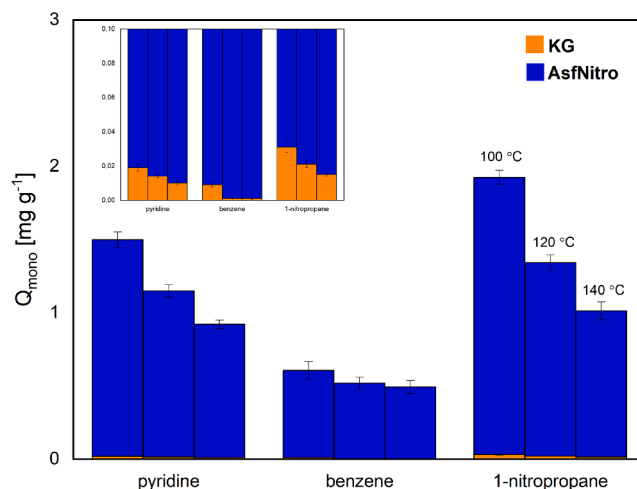

Fig. 4. Values of monolayer adsorption capacities, derived from Langmuir model.

determined by the ECP method [60]. Adsorption potential A (J mol^{-1}) is calculated by conversion of a partial pressure according to Eq. (12):

$$A = RT ln\left(\frac{P_0}{P}\right) \tag{12}$$

where P_0 is (Pa) the saturation pressure. The distribution parameter $\varnothing$ (mol mol g^{-1} J^{-1}), which is correlated with the number of adsorption sites, is calculated according to Eq. (13):

$$\varnothing = -\frac{dn}{dA} \tag{13}$$

where n (mol) is an adsorbed amount of the probe.

Fig. 5 compares the adsorption potential distribution for test probes used to determine adsorption isotherms at 100 °C, for the surface coverage in the range between 0 and 0.5. It is obvious that adsorption potential distribution of KG and AsfNitro are dissimilar, and it illustrates markedly different chemistry of the surface. The area under the curves is directly related to the uptake of the different energy sites, and it indicates that AsfNitro adsorbent has a larger number of adsorption centres on its surface, compared to KG, which are responsible for its superior adsorption capacity. For all test compounds, and both adsorbents, lower energy sites have a bigger population then the high energy.

Benzene's adsorption potentials distribution revealed that both adsorbents possess adsorption centres with similar energy, but their number on AsfNitro is greater. A sharp increase of distribution potential ($\varnothing$) on the left side (at half surface coverage) of AsfNitro's adsorption potential distribution illustrates that most of the adsorption capacity towards benzene is due to lower energy sites, that originates from aromatic rings in the structure of asphaltenes. Moreover, both distributions are rather flat, without distinct peaks in the adsorption potential range considered. It was predictable as benzene molecule is non-polar and interacts mostly by dispersive interactions.

More significant differences are observed for 1-nitropropane and pyridine adsorption potential distributions. The distributions not only indicate increased number of adsorption sites, but also a shift toward lower energy sites, for the considered range of surface's coverage (0–0.5), and multiple peaks one the AsfNitro's curves. Those peaks indicate that there are certain types of adsorption centres specific for 1-nitropropane and pyridine molecules. Insets of the Fig. 5b and c shows that surface of KG don't exhibit any specific adsorption sites for any of test compounds, at the 0–0.5 surface coverage.

Adsorbate-adsorbents interactions responsible for the observed differences in the adsorption capacity of KG and AsfNitro adsorbents, can be divided into two categories: dispersive and specific. Both were analysed by the IGC technique.
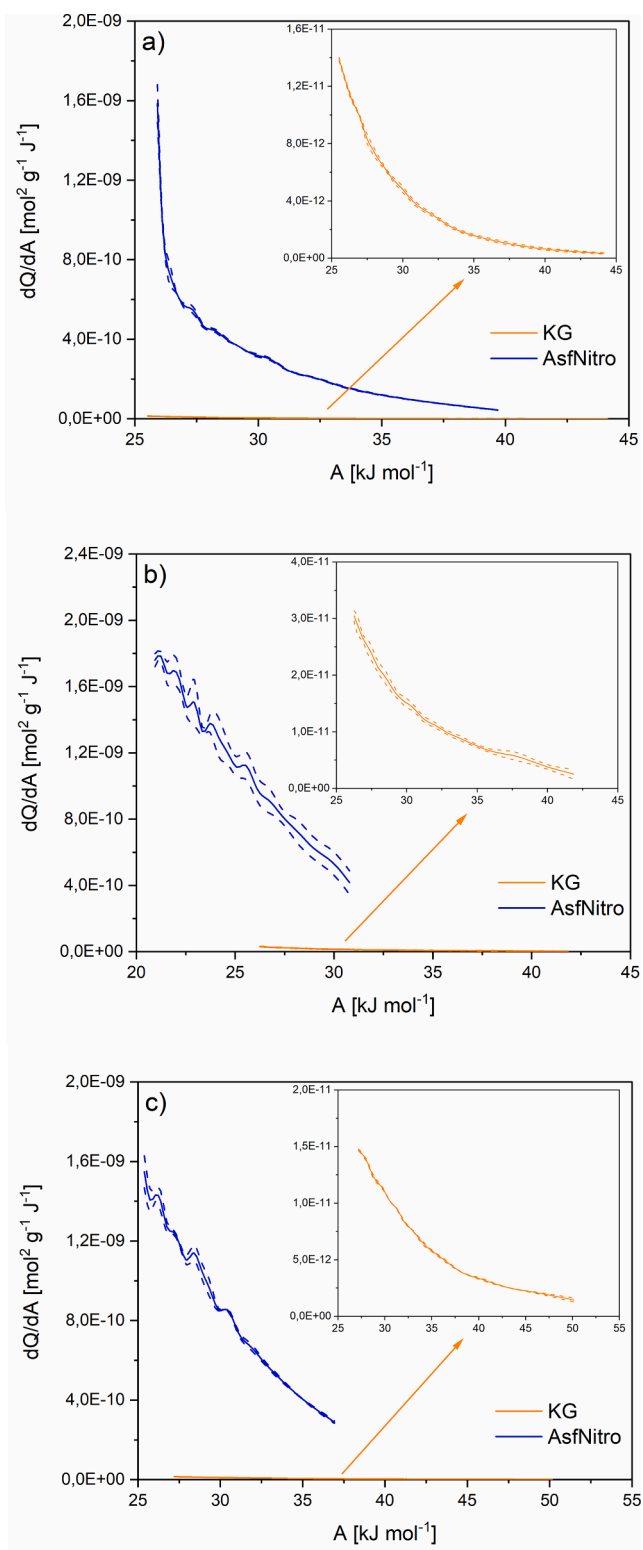
Fig. 5. Adsorption potential distribution for a) benzene, b) 1-nitropropane, c) pyridine at 100 °C.

3.2.3. Dispersive interactions

Dispersive interactions were revealed by retention of non-polar probes (e.g. n-alkanes) which interact with the surface only through dispersive interactions. Based on it, the dispersive component of the surface free energy (γ_S^D) was calculated. It is important for evaluation of activity of the surface, and is correlated with the unspecific London

interactions and heterogeneity of the surface. Generally, micro and mesoporous materials with active surface have values of γ_S^D above 200 mJ m^{-2} [60–62]. In practice, the higher the surface energy, the more interactive is the surface.

Fig. 6 compares values of γ_S^D for KG and AsfNitro and how they changes with temperature. Obtained values of γ_S^D indicate that the surface of both adsorbents (KG and AsfNitro) is relatively active, at 60 °C the value of γ_S^D is above 200 mJ m^{-2}. The result for AsfNitro is similar to previously reported, where nitrated asphaltenes were deposited on the surface of silanized support (Chromosorb W AW DCMS) [36]. In comparison to KG, dispersive interactions were only slightly enhanced by the deposition of asphaltenes on the surface of diatomaceous earth. It is in line with the small changes in ΔH_A (see Table S3) observed for n-alkanes. The value of γ_S^D for both adsorbents is linearly increasing with the temperature decrease, which is a typical behaviour for adsorbents. As the temperature decrease, the magnitude of weak London dispersion interactions is increasing because molecules of adsorbate, having less kinetic energy, reside longer on the surface of the adsorbent. Interestingly, the strength of dispersive interactions is decreasing faster, with increase of temperature, for the AsfNitro. This fact can be advantageous during thermal desorption and adsorbent regeneration as the adsorbed molecules will be more easily desorbed. This will lead to faster regeneration in lower temperature, and lower thermal stress will be imposed on adsorbent particles. Hence, particles of the AsfNitro should be more resilient to fracturing and deformations as compared to the KG. Moreover, relatively small slope of the γ_S^D versus temperature plot imply good adsorption performance stability if there will be changes of surrounding temperature.

For better understanding of results presented in the Fig. 6, comparison of γ_S^D values for different adsorbents was compiled in the Table 4. Retention of test probes (e.g. n-alkanes) strongly depends on the experimental temperature, hence there is no standard temperature used for the measurement of the γ_S^D. The experimental conditions and range of n-alkanes is selected individually for a given adsorbent in order to achieve acceptable values of retention time. Thus, the information in the Table 4 should be analysed carefully. Nevertheless, knowing that the γ_S^D is increasing with decrease of the temperature, it is apparent that the AsfNitro has a very active surface, exceeding some of the emerging adsorbents (e.g. MOFs) and comparable with carbonaceous materials (CNTs, AC). Results indicate that deposition of asphaltenes on the surface of materials is an effective method to obtain very good activity and adsorption performance.
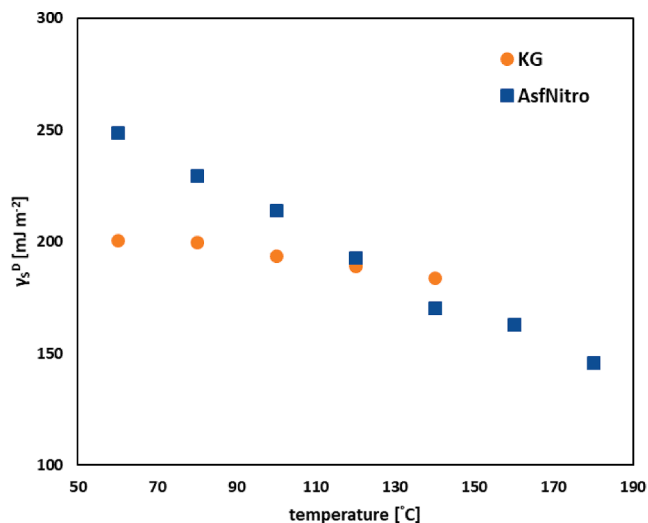

Fig. 6. Value of the dispersive component of the surface free energy γ_S^D in different temperatures for KG and AsfNitro adsorbents.

Table 4
Comparison of dispersive surface energy for various adsorbents.

Adsorbent	T [°C]	γ_S^D [mJ m^{-2}]	Reference
IRMOF	180	91	[63]
CNT	200	125	[64]
HKUST-1 (MOF)	90	144.5	[65]
AsfNitro	**80**	**229.54 ± 0.18**	**This work**
RD granular silica gel	90	93.14	[61]
SBA-16 (porous silica)	93	71,93	[66]
Maxsorb III (AC)	140	213.98	[67]
Chemviron F400	350	208.20	[60]
High surface area graphite	200	115	[68]

While the γ_S^D measured by IGC at infinite dilution is a useful parameter in materials characterization, it can be criticised for the fact that only high energy adsorption sites are probed. In some cases, as for example waste gas purification, the distribution of active sites may be more important than high energy sites. To get more insight into dispersive interactions, the adsorption potential distribution was determined for n-heptane at 100 °C. It is presented in the Fig. 7.

The adsorption potential distributions presented in the Fig. 7 were collected for the surface coverage between 0 and 0.2. This part of the studies revealed that nitrated asphaltenes are solely responsible for the adsorption potential of AsfNitro. There is a colossal increase in the number of active sites participating in the adsorption of n-heptane after coating asphaltenes on the diatomaceous earth. It shows the tremendous difference in dispersive interactions between AsfNitro and KG is not in the adsorption centres with the highest energy but in the abundance of adsorption sites with lower energy that were introduced by nitrated asphaltenes. That difference was also reflected in the n–heptane's monolayer adsorption capacity. It was over 130 times higher after deposition of asphaltenes (2.406 and 0.018 mg g^{-1}, respectively).

3.2.4. Specific interactions

As revealed by results presented in the Table S4, deposition of nitrated asphaltenes on the surface of diatomaceous earth has also a prominent effect on the specific interactions. For all test probes a decrease of ΔG_A values was observed for AsfNitro, as compared to KG adsorbent. Generally, lower value of the ΔG_A means that adsorbate is adsorbed to a greater extent. Negative values of the ΔG_A indicate that the adsorption process is thermodynamically feasible and spontaneous. For all test probes the free energy of adsorption is increasing as the temperature of measurement increase. It indicates that adsorbate molecules residence time on the surface is becoming shorter and adsorption in higher temperatures is less favourable. It is a typical phenomenon and
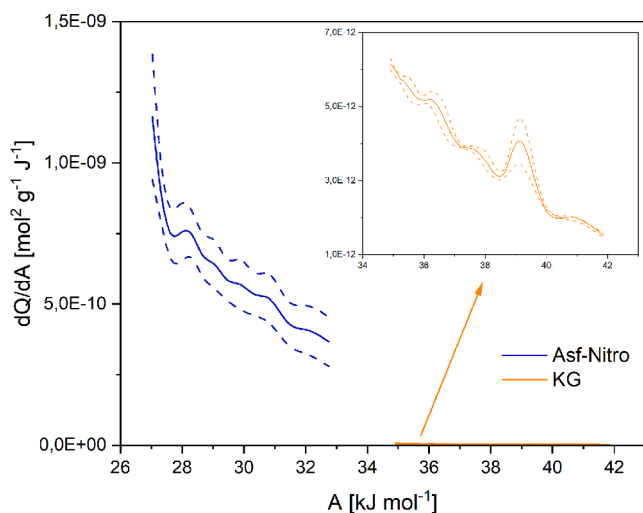

Fig. 7. Adsorption potential distribution for n-heptane at 100 °C.

a foundation of desorption process (regeneration of adsorbent). Based on ΔG_A values determined at different temperatures, the ΔH_A and ΔS_A were calculated. The obtained values are natural for adsorption process, i.e. negative values of enthalpy and entropy implies respectively that the adsorption is exothermic and that the degree of freedom decreases at the gas–solid interface. Comparison of ΔH_A for both adsorbents disclose the difference in the strength of adsorption in favour of AsfNitro adsorbent (see Table S4). Coating of KG with nitrated asphaltenes resulted in ca. 1.5–2 times increase of the ΔH_A value. The smallest change was observed for nonpolar compounds (e.g. alkanes, benzene). It is a premise that introduction of nitrated asphaltenes altered the adsorption to a greater extent through specific, than by dispersive interactions. Moreover examination of coefficient of determination (R^2) revealed that the mechanism of specific interactions of AsfNitro adsorbent may be susceptible to temperature in non-obvious manner. For KG adsorbent, value of R^2 for plot of $\frac{\Delta G_A}{T}$ versus $\frac{1}{T}$ is high for all adsorbates, whereas in case of AsfNitro very high linearity is obtained only for n-alkanes.

Table 5 compares enthalpies of adsorption, measured at infinite dilution, for selected adsorbents. Red colour indicates values lower, and green higher or equal to values calculated for material coated with nitrated asphaltenes. It is clear that AsfNitro adsorbent is superior in this respect. The adsorbents that can compete with nitrated asphaltenes are high-tech, novel materials like metal–organic frameworks (MOFs) or graphene. Moreover, the ΔH_A values of AsfNitro are above the range typically assigned to physical adsorption and fall into chemisorption range. Obtained results indicates that nitrated asphaltenes may have catalytic properties. Similar results were recently reported for oxidized asphaltenes [46]. These findings can open new paths for research about asphaltenes' properties and their novel practical applications.

Specific interactions can also be described in terms of Lewis acid-base theory. Electron donor (γ_S^-) and electron acceptor (γ_S^+) properties of the surface were revealed by measuring the retention of monopolar acid (chloroform) and monopolar base (ethyl acetate). Fig. 8 presents the ratio of γ_S^-/γ_S^+ that is describing the basicity of the surface. The higher the value, the more electrondonor the surface is. The experiment revealed the fundamentally different character of the surface of AsfNitro adsorbent, as compared to KG. The AsfNitro surface is predominantly electrondonor (basic) in the nature (the KG has mainly electron acceptor nature) that originates in the free electron rich nitro groups in the structure of nitrated asphaltenes. The specific interactions change with temperature. As it increase, the γ_S^-/γ_S^+ value decrease and the surface is becoming less electrondonor. Above 170 °C the character of the surface becomes acidic ($\gamma_S^-/\gamma_S^+ < 1$). The KG surface's character is electron acceptor in the whole range of experimental temperatures. Thus the electron rich surface of the AsfNitro adsorbent will favourably adsorb molecules with electron-acceptor capabilities.

3.3. Mechanism of adsorption.

Since BET analysis revealed that both adsorbents have similar surface areas, high adsorption capacity of AsfNitro (compared to KG) can't be ascribed to differences in specific surface area. The difference have to arise from the chemistry of the surface of AsfNitro adsorbent. In previous work [38] it was demonstrated that asphaltene-based stationary phases presents satisfactory batch-to-batch stability of adsorption properties.

Fig. 9 presents FTIR-ATR spectra of AsfNitro before and after adsorption of test probes. In the AsfNitro spectrum the presence of nitro group is manifested by three intensive bands at 1530, 1335, and 1275 cm^{-1}. They can be assigned to the asymmetrical and symmetrical aromatic C-NO$_2$ and N = O stretching, respectively [75]. Original asphaltenes have oxygen functionalities, which content may be further enhanced by acid used for nitration, as indicated by the elemental analysis results. The bands at 1720, and 1642 cm^{-2} are due to the presence of ester and amide carbonyl functionalities [76]. Bands at 2953, 2923, 2851, and 1451 cm^{-1} are attributed to the CH$_2$ and CH$_3$

Table 5
Enthalpies of adsorption ΔH_A (kJ mol^{-1}) measured by IGC-ID for different adsorbents.

	AsfNitro	AC1	ACF	PP-resin	CNTs	Graphene	HSAG300	CNT	GO	rGO	HKUST-1	Cu-BTC	IRMOF-1
acetone	78.9	33.3	61.7	58.7	49.9	–	–	–	–	–	–	70.6	74.4
DEE	101.7	–	–	–	–	–	–	–	56.1	68.4	75.4	–	84.7
THF	81.7	–	–	–	–	–	–	–	51.8	50.4	77.5	78.5	–
EtOAc	76.8	53.0	63.5	65.0	–	48.1	–	–	133.2	62.5	–	75.1	81.2
TCM	75.1	59.0	55.7	57.1	–	–	33.2	30.8	41.0	76.0	–	–	39.2
benzene	79.9	51.0	55.5	55.9	22.9	34.3	52.5	34.7	–	–	51.2	68.9	46.7
T (°C)	80–120	70–100	70–100	70–100	30–90	30–60	200–250	200–250	130–150	140–150	220–250	200–230	200
SA (m^2 g^{-1})	1.5	1068	1222	861	108	510	312	186	2	321	1168	1400	781
Ref.	This study	[69]			[70]	[71]	[64]		[72]		[73]	[74]	[63]

AC-activated carbon, ACF – activated carbon fiber, PP – porous polymeric, CNT – carbon nanotubes, HSAG – high surface area graphite, GO – graphene oxide, rGO – reduced graphene oxide, HKUST–1/Cu-BTC/IRMOF-1 – different types of metal–organic frameworks.
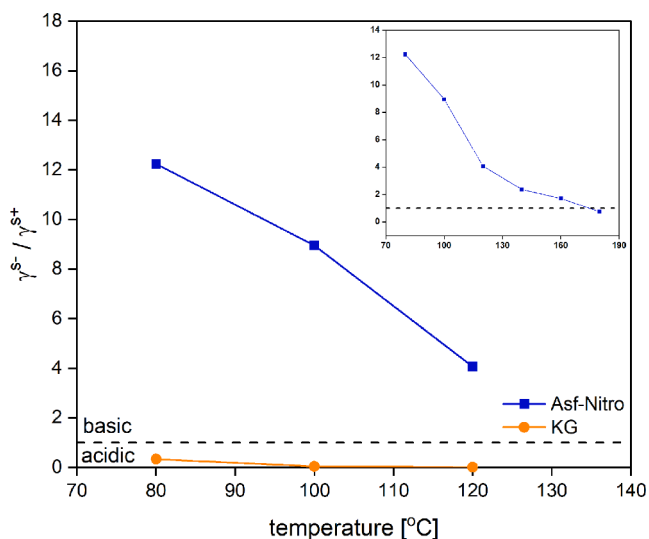

Fig. 8. Electron donor γ_S^- (basic) and electron acceptor γ_S^+ (acidic) character of KG and AsfNitro surface. The inset presents the evolution of γ_S^-/γ_S^+ in a broader range of temperature for AsfNitro.
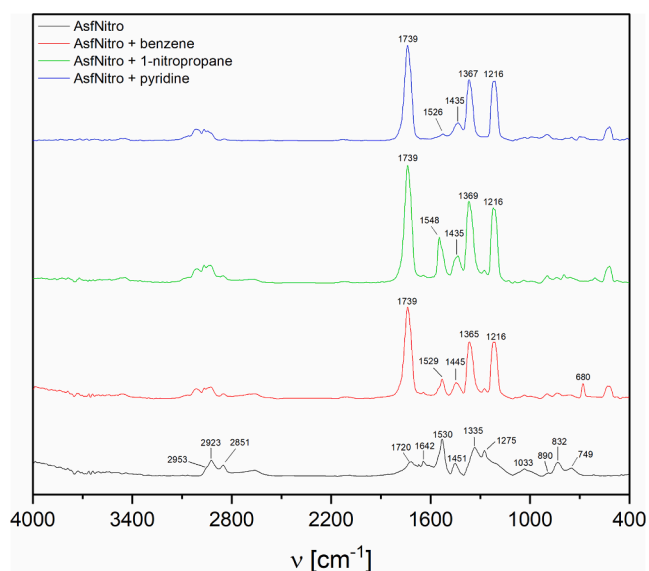

Fig. 9. FTIR-ATR spectra of AsfNitro before and after adsorption of test probes.

groups, in aliphatic chains. The signals from substituted aromatic rings, forming the backbone of asphaltenes, are visible for lower wavenumber values (bands at 890, 832, 749 cm^{-1}). The band located at 1033 may be

assigned to the sulfoxide groups, but also the C–H in-plane bending bands of aromatics occur in this region [77].

To a great extent, adsorption properties of the AsfNitro are determined by the presence of NO$_2$ groups. As a strong electron withdrawing group, it should greatly reduce the overall electron density in aromatic rings of asphaltene molecule. As a result, the aromatic core of nitrated asphaltene may act as acceptor, and electron rich nitro group as donor in donor–acceptor (charge transfer) complexes, which are partially covalent in nature, and may explain high adsorption enthalpies of test compounds [78].

The contribution of nitro group, to adsorption of VOCs is clearly manifested by changes in intensity and position of IR absorption bands [80] characteristic for NO$_2$ group, after adsorption. The band located at 1530 cm^{-1} shifted after adsorption of benzene, pyridine and 1-nitropropane to 1529, 1526, and 1548 cm^{-1}, respectively. At the same time a substantial decrease of intensity was observed for benzene and pyridine indicating interaction with –NO$_2$ group. On the other hand, for the 1-nitropropane and increased intensity was observed, that comes from –NO$_2$ groups present in the structure of 1-nitropropane molecules, adsorbed on the surface of AsfNitro.

The position of other band, originating from –NO$_2$ in AsfNitro have also changed. The band located at 1335 cm^{-1} shifted after adsorption to 1367 cm^{-1}, for all test compounds. For 1275 cm^{-1} band, a substantial decrease of intensity was observed, along with slight red-shift (1275 – 1273 cm^{-1}). Bands' position shifts are a clear indication of interaction between nitro group and adsorbates.

Molecular interaction responsible for abovementioned position shifts of absorption bands can have different nature depending on the adsorbate. For aromatic molecules they can be a n-electron and π system of the aromatic molecule interactions, or dipole interactions for 1-nitropropane molecule [80]. In case of pyridine, interaction can occur through charge transfer between –NO$_2$ group and the aromatic nitrogen [79].

Moreover, considering the structure of AsfNitro, adsorptivity of aromatic compounds (benzene, and pyridine) can be promoted by the π-π stacking interactions with the polyaromatic structure of asphaltenes. The contribution of asphaltenes' aromatic rings is proved by lower intensity of bands attributed to the substituted aromatic rings (900–750 cm^{-1} region). The stacking mechanism can be enhanced by defects in the aromatic structure of AsfNitro, introduced by the chemical modification, as carbon materials with distributed π systems possess higher adsorption capacity, than carbon materials with conjugated π systems [80,81].

Apart from specific interactions, substantial contribution to adsorption properties of AsfNitro is from dispersive interactions, which promotes adsorption of organic molecules. It is supported by the comparison of polarizability of test molecules and the adsorption capacity of AsfNitro. The capacity increase with the polarizability of the adsorbate (Figure S6, $R^2 = 0.935$) - as the polarizability increase, dispersion forces become stronger.

Dispersive interactions are also proved by contribution of alkyl chains. For benzene, and pyridine, intensity of bands attributed to CH$_2$

and CH₃ groups (2953, 2923, 2851) decreased. For 1-nitropropane increase of intensity was observed. As in the case of –NO₂ group, increase is explained by the presence of alkyl chains in adsorbed molecules.

One more distinctive change was observed on the spectra after adsorption. A strong bands at 1740, and 1216 cm⁻¹ appeared, which were assigned to the ester group (C = O, and C-O, respectively). As any of the adsorbates doesn't have carbonyl moiety in its structure, it may by an evidence of a formation of a new functional group on the surface. It is also, another signal (next to adsorption enthalpies at infinite dilution) of chemisorption on the surface of AsfNitro, and a premise for catalytic properties of nitrated asphaltenes.

4. Conclusions

This study presents an efficient adsorbent prepared by coating the porous support material (diatomaceous earth) with 10 %wt. of nitrated asphaltenes. Breakthrough curves and IGC measurements revealed that nitrated asphaltenes were exclusively responsible for the adsorption properties, and the role of the support was only to provide the surface area. Those findings can be extended to other support materials and their inherent limitations for adsorption of volatile organic compounds can be overcame.

The breakthrough experiments with selected VOCs, i.e. benzene, pyridine, and 1-nitropropane revealed significant increase in adsorption capacity after deposition of nitrated asphaltenes. Adsorption capacity of benzene calculated per gram of nitrated asphaltenes was comparable with e.g. Carboxen 1000, Tenax TA or MIL-47. Since nitrated asphaltenes are intended as the additive for coating support materials with developed surface area, the adsorption capacity of benzene was normalized by surface area of the AsfNitro. From this point of view, the AsfNitro's adsorption capacity is far more superior than for activated carbons or metal–organic frameworks. Moreover, deposition of nitrated asphaltenes was favourable for efficiency of the adsorbent. For 1-nitropropane and pyridine, the AsfNitro's bed was exhausted in 94, and 84% when breakthrough occurred - two times higher than for uncoated support material. It is certainly not without significance for the economics of the adsorption process – almost 100% of the bed was effectively used in waste gas purification. Breakthrough tests under humid conditions demonstrated that AsfNitro adsorbent is susceptible to the presence of water to the same extent as activated carbons.

IGC measurements supported the conclusion that nitrated asphaltenes are solely the source of remarkably strong interactions with adsorbates. Adsorption isotherms showed a significant increase of adsorption capacity, after coating the support with asphaltenes, that can be explained by increase of both dispersive and specific interactions – mainly of electrondonor nature. Comparison of adsorption enthalpies at infinite dilution demonstrated that activated carbons cannot compete in that matter with AsfNitro. The only comparable adsorbents (still falling behind AsfNitro) were metal–organic frameworks and graphene. Additionally, the values of adsorption enthalpies for AsfNitro indicated contribution of chemisorption to overall adsorption. This is a premise, supported by FTIR measurement, that nitrated asphaltenes may have catalytic properties. If such, than it opens a new path for research about asphaltenes' novel practical applications.

Presented results explicitly demonstrate the applicability of nitrated asphaltenes in adsorption processes and waste gas purification, and durability of the chemical modification with –NO₂ groups. Unique structure of AsfNitro is a source of various interactions that promote VOCs' adsorption, and facile coating of nitrated asphaltenes on a support, easily available in the target destination (e.g. natural clays, rocks), can be an effective procedure for risk mitigation of hazardous VOCs, accompanied by effective waste management and valorisation of a material that is considered a waste in petroleum industry.

Declaration of Competing Interest

The authors declare that they have no known competing financial interests or personal relationships that could have appeared to influence the work reported in this paper.

Appendix A. Supplementary data

Supplementary data to this article can be found online at https://doi.org/10.1016/j.cej.2021.130653.

References

[1] G. Boczkaj, P. Makoś, A. Fernandes, A. Przyjazny, New procedure for the examination of the degradation of volatile organonitrogen compounds during the treatment of industrial effluents, J. Sep. Sci. 40 (6) (2017) 1301–1309, https://doi.org/10.1002/jssc.201601237.
[2] G. Boczkaj, A. Przyjazny, M. Kamiński, Characteristics of volatile organic compounds emission profiles from hot road bitumens, Chemosphere 107 (2014) 23–30, https://doi.org/10.1016/j.chemosphere.2014.02.070.
[3] N.P.R.I. (Canada), Guide for reporting to the National Pollutant Release Inventory, 2016.
[4] European Parliament; European Council, Directive 2004/42/CE, 2004.
[5] Na Li, Qi Jiang, Fusong Wang, Peide Cui, Jun Xie, Jiashuo Li, Shaopeng Wu, Diego Maria Barbieri, Comparative assessment of asphalt volatile organic compounds emission from field to laboratory, J. Clean. Prod. 278 (2021) 123479, https://doi.org/10.1016/j.jclepro.2020.123479.
[6] C. Geng, W. Yang, X. Sun, X. Wang, Z. Bai, X. Zhang, Emission factors, ozone and secondary organic aerosol formation potential of volatile organic compounds emitted from industrial biomass boilers, J. Environ. Sci. (China) 83 (2019) 64–72, https://doi.org/10.1016/j.jes.2019.03.012.
[7] Yuxiu Zhang, Chaohai Wei, Bo Yan, Emission characteristics and associated health risk assessment of volatile organic compounds from a typical coking wastewater treatment plant, Sci. Total Environ. 693 (2019) 133417, https://doi.org/10.1016/j.scitotenv.2019.07.223.
[8] R. Tong, L. Zhang, X. Yang, J. Liu, P. Zhou, J. Li, Emission characteristics and probabilistic health risk of volatile organic compounds from solvents in wooden furniture manufacturing, J. Clean. Prod. 208 (2019) 1096–1108, https://doi.org/10.1016/j.jclepro.2018.10.195.
[9] Maria Rosa Ras, Rosa Maria Marcé, Francesc Borrull, Characterization of ozone precursor volatile organic compounds in urban atmospheres and around the petrochemical industry in the Tarragona region, Sci. Total Environ. 407 (14) (2009) 4312–4319, https://doi.org/10.1016/j.scitotenv.2009.04.001.
[10] Alex Guenther, C. Nicholas Hewitt, David Erickson, Ray Fall, Chris Geron, Tom Graedel, Peter Harley, Lee Klinger, Manuel Lerdau, W.A. Mckay, Tom Pierce, Bob Scholes, Rainer Steinbrecher, Raja Tallamraju, John Taylor, Pat Zimmerman, A global model of natural volatile organic compound emissions, J. Geophys. Res. 100 (D5) (1995) 8873, https://doi.org/10.1029/94JD02950.
[11] Y. Ren, Z. Qu, Y. Du, R. Xu, D. Ma, G. Yang, Y. Shi, X. Fan, A. Tani, P. Guo, Y. Ge, J. Chang, Air quality and health effects of biogenic volatile organic compounds emissions from urban green spaces and the mitigation strategies, Environ. Pollut. 230 (2017) 849–861, https://doi.org/10.1016/j.envpol.2017.06.049.
[12] E. Nie, G. Zheng, Z. Shao, J. Yang, T. Chen, Emission characteristics and health risk assessment of volatile organic compounds produced during municipal solid waste composting, Waste Manag. 79 (2018) 188–195, https://doi.org/10.1016/j.wasman.2018.07.024.
[13] Ruoyu Hu, Guijian Liu, Hong Zhang, Huaqin Xue, Xin Wang, Paul Kwan Sing Lam, Odor pollution due to industrial emission of volatile organic compounds: A case study in Hefei, China, J. Clean. Prod. 246 (2020) 119075, https://doi.org/10.1016/j.jclepro.2019.119075.
[14] Nicole E. Rabaud, Susan E. Ebeler, Lowell L. Ashbaugh, Robert G. Flocchini, Characterization and quantification of odorous and non-odorous volatile organic compounds near a commercial dairy in California, Atmos. Environ. 37 (7) (2003) 933–940, https://doi.org/10.1016/S1352-2310(02)00970-6.
[15] R.M. Fisher, N. Le-Minh, E.C. Sivret, J.P. Alvarez-Gaitan, S.J. Moore, R.M. Stuetz, Distribution and sensorial relevance of volatile organic compounds emitted throughout wastewater biosolids processing, Sci. Total Environ. 599–600 (2017) 663–670, https://doi.org/10.1016/j.scitotenv.2017.04.129.
[16] J. Badach, P. Kolasińska, M. Paciorek, W. Wojnowski, T. Dymerski, J. Gębicki, M. Dymnicka, J. Namieśnik, A case study of odour nuisance evaluation in the context of integrated urban planning, J. Environ. Manage. 213 (2018) 417–424, https://doi.org/10.1016/j.jenvman.2018.02.086.

[17] M. Keck, K. Mager, K. Weber, M. Keller, M. Frei, B. Steiner, S. Schrade, Odour impact from farms with animal husbandry and biogas facilities, Sci. Total Environ. 645 (2018) 1432–1443, https://doi.org/10.1016/j.scitotenv.2018.07.182.

[18] F.I. Khan, A. Kr, A.K. Ghoshal Ghoshal, Removal of volatile organic compounds from polluted air, J. Loss Prev. Process Ind. 13 (2000) 527–545, https://doi.org/10.1016/S0950-4230(00)00007-3.

[19] Maurizio Sansotera, Sina Geran Malek Kheyli, Alberto Baggioli, Claudia L. Bianchi, Maria Pia Pedeferri, Maria Vittoria Diamanti, Walter Navarrini, Absorption and photocatalytic degradation of VOCs by perfluorinated ionomeric coating with TiO2 nanopowders for air purification, Chem. Eng. J. 361 (2019) 885–896, https://doi.org/10.1016/j.cej.2018.12.136.

[20] C. Yang, G. Miao, Y. Pi, Q. Xia, J. Wu, Z. Li, J. Xiao, Abatement of various types of VOCs by adsorption/catalytic oxidation: A review, Chem. Eng. J. 370 (2019) 1128–1153, https://doi.org/10.1016/j.cej.2019.03.232.

[21] Xin Li, Jie Ma, Xiang Ling, Design and dynamic behaviour investigation of a novel VOC recovery system based on a deep condensation process, Cryogenics (Guildf). 107 (2020) 103060, https://doi.org/10.1016/j.cryogenics.2020.103060.

[22] M.S. Kamal, S.A. Razzak, M.M. Hossain, Catalytic oxidation of volatile organic compounds (VOCs) - A review, Atmos. Environ. 140 (2016) 117–134, https://doi.org/10.1016/j.atmosenv.2016.05.031.

[23] M. Gospodarek, P. Rybarczyk, B. Szulczyński, J. Gębicki, Comparative evaluation of selected biological methods for the removal of hydrophilic and hydrophobic odorous VOCs from air, Processes. 7 (2019) 12–15, https://doi.org/10.3390/pr7040187.

[24] M. Tomatis, M.T. Moreira, H. Xu, W. Deng, J. He, A.M. Parvez, Removal of VOCs from waste gases using various thermal oxidizers: A comparative study based on life cycle assessment and cost analysis in China, J. Clean. Prod. 233 (2019) 808–818, https://doi.org/10.1016/j.jclepro.2019.06.131.

[25] M.F. Mustafa, X. Fu, Y. Liu, Y. Abbas, H. Wang, W. Lu, Volatile organic compounds (VOCs) removal in non-thermal plasma double dielectric barrier discharge reactor, J. Hazard. Mater. 347 (2018) 317–324, https://doi.org/10.1016/j.jhazmat.2018.01.021.

[26] Xiuquan Li, Li Zhang, Zhongqing Yang, Peng Wang, Yunfei Yan, Jingyu Ran, Adsorption materials for volatile organic compounds (VOCs) and the key factors for VOCs adsorption process: A review, Sep. Purif. Technol. 235 (2020) 116213, https://doi.org/10.1016/j.seppur.2019.116213.

[27] H. Sui, P. An, X. Li, S. Cong, L. He, Removal and recovery of o-xylene by silica gel using vacuum swing adsorption, Chem. Eng. J. 316 (2017) 232–242, https://doi.org/10.1016/j.cej.2017.01.061.

[28] X. Zhang, B. Gao, A.E. Creamer, C. Cao, Y. Li, Adsorption of VOCs onto engineered carbon materials: A review, J. Hazard. Mater. 338 (2017) 102–123, https://doi.org/10.1016/j.jhazmat.2017.05.013.

[29] G. Zhang, Y. Liu, S. Zheng, Z. Hashisho, Adsorption of volatile organic compounds onto natural porous minerals, J. Hazard. Mater. 364 (2019) 317–324, https://doi.org/10.1016/j.jhazmat.2018.10.031.

[30] J.E. Szulejko, K.H. Kim, J. Parise, Seeking the most powerful and practical real-world sorbents for gaseous benzene as a representative volatile organic compound based on performance metrics, Sep. Purif. Technol. 212 (2019) 980–985, https://doi.org/10.1016/j.seppur.2018.11.001.

[31] Mei-syue Li, Siang Chen Wu, Yang-hsin Shih, Characterization of volatile organic compound adsorption on multiwall carbon nanotubes under different levels of relative humidity using linear solvation energy relationship, J. Hazard. Mater. 315 (2016) 35–41, https://doi.org/10.1016/j.jhazmat.2016.04.004.

[32] L. Yu, L. Wang, W. Xu, L. Chen, M. Fu, J. Wu, D. Ye, Adsorption of VOCs on reduced graphene oxide, J. Environ. Sci. (China) 67 (2017) 171–178, https://doi.org/10.1016/j.jes.2017.08.022.

[33] K. Vellingiri, J.E. Szulejko, P. Kumar, E.E. Kwon, K.H. Kim, A. Deep, D. W. Boukhvalov, R.J.C. Brown, Metal organic frameworks as sorption media for volatile and semi-volatile organic compounds at ambient conditions, Sci. Rep. 6 (2016) 27813, https://doi.org/10.1038/srep27813.

[34] R.R. Gil, B. Ruiz, M.S. Lozano, M.J. Martín, E. Fuente, VOCs removal by adsorption onto activated carbons from biocollagenic wastes of vegetable tanning, Chem. Eng. J. 245 (2014) 80–88, https://doi.org/10.1016/j.cej.2014.02.012.

[35] Alba Anfruns, María J. Martin, Miguel A. Montes-Morán, Removal of odourous VOCs using sludge-based adsorbents, Chem. Eng. J. 166 (3) (2011) 1022–1031, https://doi.org/10.1016/j.cej.2010.11.095.

[36] M. Plata-Gryl, M. Momotko, S. Makowiec, G. Boczkaj, Highly effective asphaltene-derived adsorbents for gas phase removal of volatile organic compounds, Sep. Purif. Technol. 224 (2019) 315–321, https://doi.org/10.1016/j.seppur.2019.05.041.

[37] Maksymilian Plata-Gryl, Malwina Momotko, Sławomir Makowiec, Grzegorz Boczkaj, Application of cyanated asphaltenes in gas-phase adsorption processes for removal of volatile organic compounds, Chem. Pap. 74 (3) (2020) 995–1008, https://doi.org/10.1007/s11696-019-00938-z.

[38] Grzegorz Boczkaj, Malwina Momotko, Dorota Chruszczyk, Andrzej Przyjazny, Marian Kamiński, Novel stationary phases based on asphaltenes for gas chromatography, J. Sep. Sci. 39 (13) (2016) 2527–2536, https://doi.org/10.1002/jssc.201600183.

[39] N.K. Rajan, V. Selvavathi, B. Sairam, J.M. Krishnan, Influence of asphaltenes on the rheological properties of blended paving asphalts, Pet. Sci. Technol. 28 (4) (2010) 331–350, https://doi.org/10.1080/10916460802640282.

[40] A. Seitllari, Y.S. Kumbargeri, K.P. Biligiri, I. Boz, A soft computing approach to predict and evaluate asphalt mixture aging characteristics using asphaltene as a performance indicator, Mater. Struct. Constr. 52 (2019) 1–11, https://doi.org/10.1617/s11527-019-1402-5.

[41] Chen Wang, Tiantai Li, Hui Gao, Jinsheng Zhao, Yuan Gao, Quantitative study on the blockage degree of pores due to asphaltene precipitation in low-permeability reservoirs with NMR technique, Elsevier B.V. 163 (2018) 703–711, https://doi.org/10.1016/j.petrol.2017.11.021.

[42] K. Akbarzadeh, A. Hammami, A. Kharrat, D. Zhang, S. Allenson, J. Creek, S. Kabir, A. Jamaluddin, A.G. Marshall, R.P. Rodgers, O.C. Mullins, T. Solbakken, Asphaltenes—problematic but rich in potential, Oilf, Rev. (2007) 22–43.

[43] Oliver C. Mullins, The asphaltenes, Annu. Rev. Anal. Chem. 4 (1) (2011) 393–418, https://doi.org/10.1146/annurev-anchem-061010-113849.

[44] Henning Groenzin, Oliver C. Mullins, Molecular size and structure of asphaltenes from various sources, Energy Fuels. 14 (3) (2000) 677–684, https://doi.org/10.1021/ef990225z.

[45] Bruno Schuler, Gerhard Meyer, Diego Peña, Oliver C. Mullins, Leo Gross, Unraveling the Molecular Structures of Asphaltenes by Atomic Force Microscopy, J. Am. Chem. Soc. 137 (31) (2015) 9870–9876, https://doi.org/10.1021/jacs.5b04056.

[46] H. Jung, C.W. Bielawski, Asphaltene oxide promotes a broad range of synthetic transformations, Commun. Chem. 2 (2019) 1–9, https://doi.org/10.1038/s42004-019-0214-4.

[47] Kirill Fedorov, Maksymilian Plata-Gryl, Javed Ali Khan, Grzegorz Boczkaj, Ultrasound-assisted heterogeneous activation of persulfate and peroxymonosulfate by asphaltenes for the degradation of BTEX in water, J. Hazard. Mater. 397 (2020) 122804, https://doi.org/10.1016/j.jhazmat.2020.122804.

[48] M. Plata-Gryl, C. Jungnickel, G. Boczkaj, An improved scalable method of isolating asphaltenes, J. Pet. Sci. Eng. 167 (2018) 608–614, https://doi.org/10.1016/j.petrol.2018.04.039.

[49] National Institute for Occupational Safety and Health, Pocket Guide to Chemical Hazards, 2007.

[50] R: A language and environment for statistical computing, (2008). http://www.r-project.org.

[51] T.V. Elzhov, K.M. Mullen, A.-N. Spiess, B. Bolker, minpack.lm: R Interface to the Levenberg-Marquardt nonlinear least-squares algorithm found in MINPACK, plus support for bounds, (2016).

[52] M. Al-Ghouti, M.A.M. Khraisheh, M.N.M. Ahmad, S. Allen, Thermodynamic behaviour and the effect of temperature on the removal of dyes from aqueous solution using modified diatomite: A kinetic study, J. Colloid Interface Sci. 287 (1) (2005) 6–13, https://doi.org/10.1016/j.jcis.2005.02.002.

[53] Wen-Tien Tsai, Chi-Wei Lai, Kuo-Jong Hsien, Characterization and adsorption properties of diatomaceous earth modified by hydrofluoric acid etching, J. Colloid Interface Sci. 297 (2) (2006) 749–754, https://doi.org/10.1016/j.jcis.2005.10.058.

[54] Khim Hoong Chu, Breakthrough curve analysis by simplistic models of fixed bed adsorption: In defense of the century-old Bohart-Adams model, Chem. Eng. J. 380 (2020) 122513, https://doi.org/10.1016/j.cej.2019.122513.

[55] Andrei Veksha, Eiji Sasaoka, Md. Azhar Uddin, The influence of porosity and surface oxygen groups of peat-based activated carbons on benzene adsorption from dry and humid air, Carbon N. Y. 47 (10) (2009) 2371–2378, https://doi.org/10.1016/j.carbon.2009.04.028.

[56] I. Langmuir, Adsorption of gases on plain surfaces of glass mica platinum, J. Am. Chem. Soc. 40 (1918) 1361–1403.

[57] M. Jaroniec, Adsorption on heterogeneous surfaces: The exponential equation for the overall adsorption isotherm, Surf. Sci. 50 (2) (1975) 553–564, https://doi.org/10.1016/0039-6028(75)90044-8.

[58] Thio Christine Chandra, M.M. Mirna, Y. Sudaryanto, S. Ismadji, Adsorption of basic dye onto activated carbon prepared from durian shell: Studies of adsorption equilibrium and kinetics, Chem. Eng. J. 127 (1-3) (2007) 121–129, https://doi.org/10.1016/j.cej.2006.09.011.

[59] S.J. Gregg, K. Sing, Adsorption, surface area and porosity, Academic Press, Michigan, 1982.

[60] Frank Thielmann, Introduction into the characterisation of porous materials by inverse gas chromatography, J. Chromatogr. A 1037 (1-2) (2004) 115–123, https://doi.org/10.1016/j.chroma.2004.03.060.

[61] M.L. Palash, Animesh Pal, Tahmid Hasan Rupam, Byung-Duck Park, Bidyut Baran Saha, Surface energy characterization of different particulate silica gels at infinite dilution, Colloids Surfaces A Physicochem. Eng. Asp. 603 (2020) 125209, https://doi.org/10.1016/j.colsurfa.2020.125209.

[62] Pirre P. Ylä-Mäihäniemi, Jerry Y.Y. Heng, Frank Thielmann, Daryl R. Williams, Inverse gas chromatographic method for measuring the dispersive surface energy distribution for particulates, Langmuir 24 (17) (2008) 9551–9557, https://doi.org/10.1021/la801676n.

[63] Matthew T. Luebbers, Tianjiao Wu, Lingjuan Shen, Richard I. Masel, Trends in the adsorption of volatile organic compounds in a large-pore metal-organic framework, IRMOF-1, Langmuir 26 (13) (2010) 11319–11329, https://doi.org/10.1021/la100563r.

[64] Eva Díaz, Salvador Ordóñez, Aurelio Vega, Adsorption of volatile organic compounds onto carbon nanotubes, carbon nanofibers, and high-surface-area graphites, J. Colloid Interface Sci. 305 (1) (2007) 7–16, https://doi.org/10.1016/j.jcis.2006.09.036.

[65] A.S. Münch, F.O.R.L. Mertens, Investigation of n-alkane adsorption on HKUST-1 and determination of intrinsic interfacial energy contributions, Microporous Mesoporous Mater. 270 (2018) 180–188, https://doi.org/10.1016/j.micromeso.2018.05.012.

[66] M. Rückriem, A. Inayat, D. Enke, R. Gläser, W.-D. Einicke, R. Rockmann, Inverse gas chromatography for determining the dispersive surface energy of porous silica, Colloids Surfaces A Physicochem. Eng. Asp. 357 (1-3) (2010) 21–26, https://doi.org/10.1016/j.colsurfa.2009.12.001.

[67] A. Pal, A. Kondor, S. Mitra, K. Thu, S. Harish, B.B. Saha, On surface energy and acid–base properties of highly porous parent and surface treated activated carbons using inverse gas chromatography, J. Ind. Eng. Chem. 69 (2019) 432–443, https://doi.org/10.1016/j.jiec.2018.09.046.

[68] Montserrat R. Cuervo, Esther Asedegbega-Nieto, Eva Díaz, Salvador Ordóñez, Aurelio Vega, Ana Belén Dongil, Inmaculada Rodríguez-Ramos, Modification of the adsorption properties of high surface area graphites by oxygen functional groups, Carbon N. Y. 46 (15) (2008) 2096–2106, https://doi.org/10.1016/j.carbon.2008.08.025.

[69] Huijuan Liu, Bowen Xu, Keyan Wei, Yansong Yu, Chao Long, Adsorption of low-concentration VOCs on various adsorbents: Correlating partition coefficient with surface energy of adsorbent, Sci. Total Environ. 733 (2020) 139376, https://doi.org/10.1016/j.scitotenv.2020.139376.

[70] Yang-hsin Shih, Mei-syue Li, Adsorption of selected volatile organic vapors on multiwall carbon nanotubes, J. Hazard. Mater. 154 (1-3) (2008) 21–28, https://doi.org/10.1016/j.jhazmat.2007.09.095.

[71] Petr Lazar, František Karlický, Petr Jurečka, Mikuláš Kocman, Eva Otyepková, Klára Šafářová, Michal Otyepka, Adsorption of small organic molecules on graphene, J. Am. Chem. Soc. 135 (16) (2013) 6372–6377, https://doi.org/10.1021/ja403162r.

[72] H. Grajek, J. Jonik, L. Rutkowski, M. Purchała, T. Wawer, The optimisation of chromatographic conditions for determination of acceptor-donor properties of graphene oxide and reduced graphene oxide, Acta Innov. 26 (2018) 5–20.

[73] Alexander S. Münch, Florian O.R.L. Mertens, The Lewis acidic and basic character of the internal HKUST-1 surface determined by inverse gas chromatography, CrystEngComm 17 (2) (2015) 438–447, https://doi.org/10.1039/C4CE01327A.

[74] Giselle Autié-Castro, Edilso Reguera, Celio L. Cavalcante, Antonio S. Araujo, Enrique Rodríguez-Castellón, Surface acid-base properties of Cu-BTC and Fe-BTC MOFs. An inverse gas chromatography and n-butylamine thermo desorption study, Inorganica Chim. Acta. 507 (2020) 119590, https://doi.org/10.1016/j.ica.2020.119590.

[75] M.N. Siddiqui, I.W. Kazi, Chlorination, nitration, and amination reactions of asphaltene, Pet. Sci. Technol. 32 (24) (2014) 2987–2994, https://doi.org/10.1080/10916466.2014.924528.

[76] J. Douda, M.E. Llanos, R. Alvarez, J. Navarrete Bolaños, Structure of Maya asphaltene−resin complexes through the analysis of soxhlet extracted fractions, Energy Fuels 18 (3) (2004) 736–742, https://doi.org/10.1021/ef034057t.

[77] Morteza Asemani, Ahmad Reza Rabbani, Detailed FTIR spectroscopy characterization of crude oil extracted asphaltenes: Curve resolve of overlapping bands, J. Pet. Sci. Eng. 185 (2020) 106618, https://doi.org/10.1016/j.petrol.2019.106618.

[78] L. Emmett, G.M. Prentice, G.D. Pantoş, Donor-acceptor interactions in chemistry, Annu. Reports Prog. Chem. - Sect. B. 109 (2013) 217–234, https://doi.org/10.1039/c3oc90004e.

[79] Sandeep Kumar, D.R. Sharma, N. Thakur, N.S. Negi, V.S. Rangra, Molecular associations in binary mixture of pyridine and nitrobenzene in benzene solution using microwave absorption data, Z. Phys. Chem. 219 (12_2005) (2005) 1649–1654, https://doi.org/10.1524/zpch.2005.219.12.1649.

[80] Xiaoxiao Chen, Baoliang Chen, Macroscopic and spectroscopic investigations of the adsorption of nitroaromatic compounds on graphene oxide, reduced graphene oxide, and graphene nanosheets, Environ. Sci. Technol. 49 (10) (2015) 6181–6189, https://doi.org/10.1021/es5054946.

[81] Jun Wang, Baoliang Chen, Baoshan Xing, Wrinkles and folds of activated graphene nanosheets as fast and efficient adsorptive sites for hydrophobic organic contaminants, Environ. Sci. Technol. 50 (7) (2016) 3798–3808, https://doi.org/10.1021/acs.est.5b04865.